PAF1C-driven restoration of RNAPII elongation after DNA damage occurs independently of transcription-associated histone mark deposition

Janne J.M. van Schie[1], Bram A.F.J. de Groot[1], Martijn S. Luijsterburg[1*]

[1] Department of Human Genetics, Leiden University Medical Center, Leiden, The Netherlands

Corresponding author:

Martijn S. Luijsterburg (m.luijsterburg@lumc.nl)

Abstract

DNA lesions block the progression of RNA polymerase II (RNAPII) during transcription, impeding gene expression and threatening genome integrity. When RNAPII stalls on transcription-blocking lesions, the transcription-coupled DNA repair pathway is activated to remove the DNA damage. Following DNA repair, efficient transcription restart depends on the PAF1 elongation complex (PAF1C). PAF1C contributes to deposition of transcription-associated histone marks, including H2B-K120$_{Ub}$, H3K4me$_3$ and H3K79me$_2$. These marks are enriched at actively transcribed genes and have been associated with regulation of post-repair transcription restart. Here, we show that the H2B-K120 E3 ubiquitin ligase RNF20/RNF40, the H3K4-methyltransferase SET1/COMPASS complex, and the H3K79-methyltransferase DOT1L are dispensable for transcription restart. Moreover, levels of H2B-K120$_{Ub}$ and H3K4me$_3$ do not correlate with transcription restoration following DNA damage. Additionally, we observe that, unlike PAF1, the dissociable PAF1C subunit RTF1, while stimulating H2B-K120$_{Ub}$ and H3K4me$_3$, does not play a role in transcription restart. Together, these data suggest that transcription restoration after DNA damage is stimulated by the PAF1C elongation complex, independently of transcription-associated histone mark deposition.

Introduction

The presence of DNA damage in the transcribed strand presents a major obstacle to transcription, leading to persistent stalling of RNA polymerase II (RNAPII) at bulky DNA lesions. This stalling is highly toxic and triggers a genome-wide transcriptional arrest. While DNA lesions lead to the direct stalling of elongating RNAPII *in cis*, there is also a regulated inhibition of transcription initiation *in trans* via the stress-induced repressor ATF3 and RNAPII degradation [1-4]. Overcoming transcriptional arrest and restoring transcription after DNA repair is essential for maintaining proper gene expression and cellular homeostasis.

To remove transcription-blocking DNA lesions, cells rely on the transcription-coupled DNA repair (TCR) pathway. TCR is initiated by the coordinated recruitment of the TCR-specific proteins CSB, CSA, UVSSA and STK19 to DNA damage-stalled RNAPII assisted by elongation factor ELOF1 [5-11]. Together, these factors promote the recruitment of the TFIIH complex to damage-stalled RNAPII, leading to either backtracking or displacement of RNAPII to facilitate access to downstream repair proteins. Subsequently, general NER proteins, such as XPA, RPA, and the endonucleases XPG and ERCC1-XPF, coordinate dual incision around the lesion to remove the damaged DNA strand, followed by gap fill DNA synthesis and ligation. Mutations in TCR components CSB and CSA cause Cockayne syndrome, a progeroid disorder characterized by severe developmental and neurological dysfunction [12,13].

While the removal of DNA lesions by TCR is essential, it is not sufficient for transcription restart. TCR involves displacement of RNAPII from the damaged DNA template [14-17], followed by transcription restart from gene promoters. Post-repair transcription restart requires the alleviation of ATF3-mediated transcriptional repression at gene promoters by CSB- and CSA-mediated degradation of ATF3 [1,18]. Furthermore, chromatin remodeling has been implicated in post-repair transcriptional restart [19]. While these observations suggest post-restart repair pathways are at least partially distinct from general transcription requirements, the precise mechanisms driving transcription recovery and their coordination with TCR-mediated repair remain to be fully elucidated.

The PAF1 subunit of the RNA polymerase II-associated factor complex (PAF1C) has emerged as a critical component in regulating transcriptional restart following genotoxic stress [20]. The PAF1C, composed of subunits CTR9, PAF1, LEO1, CDC73, SKI8 and the loosely associated subunit RTF1, localizes to actively transcribed genes through its association with RNAPII to regulate transcription elongation, promoter-proximal pausing, and the deposition of histone modifications [21-26]. Which functions of the PAF1C contribute to transcription restart and whether subunits other than PAF1 are required for restart is currently unknown.

PAF1C recruits the ubiquitin conjugase (E2) RAD6A (UBE2A) and the RING-type E3 ubiquitin ligase complex RNF20-RNF40 to RNAPII to co-transcriptionally mono-ubiquitylate histone H2B at lysine 120 ($H2BK120_{ub}$) [27,28]. In both yeast and human, this modification stimulates the subsequent deposition of H3K4 trimethylation ($H3K4_{me3}$) by the SET1/COMPASS complex and H3K79 dimethylation ($H3K79_{me2}$) by DOT1L [28-33]. Thereby, PAF1C stimulates the deposition of histone marks $H2BK120_{Ub}$, $H3K4_{me3}$, and $H3K79_{me2}$ [34] which are all associated with active transcription [35,36]. $H3K4_{me3}$ is mainly enriched close to

promoters and correlates with transcription initiation and promoter proximal pause release [37,38]. H2BK120$_{Ub}$ and H3K79$_{me2}$ are enriched in gene bodies of active genes, and have both been linked to transcription elongation and the DNA damage response [39-41]. In addition, H2BK120$_{ub}$, H3K4$_{me3}$ and H3K79$_{me2}$ have been associated with restoring post-repair transcription restart. UV-induced H3K4 methylation facilitates transcriptional reactivation in *C. elegans* [42], while DOT1L-mediated H3K79 methylation contributes to transcription restart in mouse cells [43]. Furthermore, H2BK120$_{ub}$ levels are reduced after UV damage [20,44]. Together, these findings suggest a potential interplay between transcription-associated histone modifications and transcription recovery [20], but this has not been directly assessed in human cells.

In this study, we found that transcription-associated histone modifications H2BK120$_{Ub}$, H3K4$_{me3}$, and H3K79$_{me}$ are dispensable for transcriptional recovery following genotoxic stress. Additionally, unlike PAF1, the dissociable PAF1C subunit RTF1, while stimulating H2B-K120$_{Ub}$ and H3K4$_{me3}$, does not play a role in transcription restart. Together, our work suggests that restoration of transcription following DNA damage depends on the ability of PAF1C to directly stimulate processive RNAPII elongation in a manner that is independent of the deposition of transcription-associated histone marks.

Results

DOT1L and H3K79 methylation are redundant for transcription restart following DNA damage

H3K79$_{me2}$ is a histone mark enriched in gene bodies of actively transcribed genes and correlates with high RNAPII elongation rates [41]. However, loss of H3K79$_{me2}$ does not seem to impact transcription elongation rates [45,46], and only causes minor changes in gene expression [47,48]. H3K79 methylation has been linked with transcription initiation [46], but the exact contribution of H3K79$_{me2}$ in transcription remains unclear [41]. Previous work has shown that H3K79$_{me2}$ facilitates transcription restart after genotoxic stress in mouse cells, possibly by opening chromatin structure to allow reactivation of RNAPII by facilitating transcription initiation [43]. Since differences in chromatin requirements for TCR between mouse and human cells have been observed before [49], we decided to test the dependence of transcription restart after DNA damage repair on H3K79$_{me2}$. To do so, we inhibited DOT1L, the only known methyltransferase of H3K79, with DOT1L inhibitor Pinometostat (DOT1Li) in human RPE1-hTERT cells. Because of the lack of an obvious H3K79 demethylase [41], reduction of H3K79$_{me2}$ seems instead to depend on histone replacement or dilution through cell division [50]. Consequently, H3K79$_{me2}$ has a relatively long half-life (multiple days) [51], which in itself makes it an unlikely candidate to dynamically respond to transcription-blocking DNA damage. To test the contribution of H3K79$_{me2}$, we treated cells for 7 days with DOT1Li, which resulted in a complete loss of H3K79$_{me2}$ as detected by western blot analysis (Fig 1A) and performed recovery of RNA synthesis (RRS) assays after UV-induced DNA damage. In all conditions, a drop of RNA synthesis was observed 3h after UV exposure. As expected, TCR-deficient CSB-KO cells were unable to recover RNA synthesis after 24h. In contrast, nascent RNA synthesis in wild-type (WT) cells treated with DOT1Li recovered to levels similar to untreated WT cells (Fig 1B). Because incomplete inhibition of H3K79 methylation or H3K79$_{me2}$-independent DOT1L functions [45] cannot be excluded using DOT1Li, we also

generated two clonal DOT1L-KO cell lines using two different crRNAs targeting exon 2 and exon 5, respectively. Isolated DOT1L-KO clones had no detectable DOT1L protein or H3K79$_{me2}$ (Fig 1C), and showed comparable levels of nascent transcription in unirradiated cells (Fig 1D). Similar to the cells treated with DOT1Li, also DOT1L-KO cells recovered nascent transcription like WT cells 24h after UV irradiation (Fig 1E). These observations show that DOT1L and H3K79 methylation are dispensable for transcription restart following genotoxic stress in human RPE1 cells.

The SET1 complex and H3K4 trimethylation are dispensable for transcription restart

H3K4$_{me3}$ is enriched near promoters and is believed to aid transcription initiation and release of promoter proximally paused RNAPII [37,38]. Consequently, RNAPII restart from promoters after DNA damage is repaired may therefore depend on H3K4$_{me3}$. The deposition of H3K4$_{me3}$ is mediated by the SET1 histone methyltransferase complexes. The H3K4 methyltransferase activities of all SET1 complexes depend on the shared WRAD complex, consisting of core subunits, WDR5, RBBP5, ASH2L and DPY30 [52]. To test H3K4$_{me3}$ involvement in transcription restart after UV, we depleted the shared core subunit RBBP5. Because the SET1 complex is essential for cell viability, likely due to its central role in transcriptional regulation [52], we were unable to generate viable RBBP5-KO clones. Instead, we acutely depleted RBBP5 using CRISPR/Cas9 and performed our assays after 5 days, when cells are still viable but have completely lost detectable levels of H3K4$_{me3}$ (Fig 2A). We subsequently measured nascent transcription levels by 5-ethynyl-uridine (5-EU) incorporation while at the same time co-staining for H3K4$_{me3}$ (Fig 2B). This approach confirmed the loss of H3K4$_{me3}$ (defined as H3K4$_{me3}$ levels lower than 0.2 relative to WT, cells depicted as pink dots) in around 90% of crRBBP5-transfected cells. However, near-complete loss of H3K4$_{me3}$ in RBBP5-depleted cells did not affect the levels of nascent transcription when compared to control cells (Fig 2C). We next performed RRS assays while also co-staining for H3K4$_{me3}$ (Fig 2D-E). While cells acutely depleted for TCR factor CSA were unable to recover RNA synthesis 24h after UV irradiation, RBBP5-depleted cells recovered like WT cells (Fig 2D). The levels of H3K4$_{me3}$ were not decreased at 3h after UV irradiation in cells transfected with negative control (NC) or CSA crRNAs when nascent transcription is reduced by ~80% (Fig 2D). Also in CSA-depleted cells at 24h, which fail to recover transcription and remain to have very low nascent RNA synthesis levels, this does not result in differences in H3K4$_{me3}$ levels. Finally, RBBP5-depleted cells at 24h after UV, while being devoid of H3K4$_{me3,}$ showed normal recovery of nascent transcription (Fig 2D). Together, this shows that the SET1 complex and H3K4$_{me3}$ are not require for the immediate restart of transcription following the repair of transcription-blocking DNA damage.

H2BK120 ubiquitination and RNF20 are not essential for transcription restart

H2BK120$_{Ub}$ is a co-transcriptionally deposited histone mark that is enriched within gene bodies of actively transcribed genes [28]. H2BK120$_{Ub}$ has been ascribed multiple functions in the DNA damage response [40]. Furthermore, levels of H2BK120$_{Ub}$ were shown to decrease following UV-induced DNA damage [20,44], suggesting a potential correlation, although not necessarily causal, between transcription restart after UV and this histone mark. H2BK120$_{Ub}$ is deposited by the E2 conjugase RAD6 together with the heterodimeric E3 ligase RNF20-RNF40, which is essential for cellular viability. To test whether H2BK120$_{Ub}$ contributes to recovery of transcription after genotoxic stress, we acutely depleted RNF20 using crRNF20 transfection together with Cas9 activation, which resulted in a strong reduction in H2B-K120$_{Ub}$ within 5 days following transfection(Fig 3A-C). More than 70% of RNF20-depleted

cells had H2BK120$_{ub}$ levels of less than 0.2 relative to cells transfected with a control (NC) crRNA (cells depicted as purple dots). Cells depleted for RNF20 were still able to normally recover RNA synthesis after UV (Fig 3D), suggesting that H2BK120$_{ub}$ is dispensable for transcription recovery after UV. In line with previous results [20,44], H2BK120$_{Ub}$ levels dropped after UV irradiation, dropping concomitantly with the reduction in transcription observed at the 3h post-UV timepoint (Fig 3C). However, when transcription recovered in control cells 24h after UV irradiation, H2BK120$_{Ub}$ levels were still not fully recovered. Together, this shows that H2BK120$_{Ub}$ and RNF20 are not essential to restart transcription after UV-induced DNA damage. Rather, these findings suggest that H2BK120$_{Ub}$ levels drop as a result of decreased transcription after UV, while restoring H2BK120$_{Ub}$ levels after UV lags behind RNAPII elongation and is substantially slower than the actual restart of transcription.

Core PAF1C subunits PAF1 and CTR9, but not subunit RTF1, is required for transcription restart

Since both PAF1 and RTF1 were found to physically interact with RAD6A/RNF20-RNF40 to stimulate H2BK120 ubiquitylation [27,28,33] and in turn H2BK120$_{ub}$ stimulates H3K4$_{me3}$ and H3K79$_{me2}$ deposition, we decided to test levels of these marks after depletion of PAF1 and RTF1. Depletion of PAF1 and more prominently for RTF1 resulted in a pronounced drop in H2B-K120$_{ub}$ levels (Fig. 4A-B). In addition, levels of H3K4$_{me3}$ were also strongly decreased, particularly in RTF1-depleted cells. RTF1 or PAF1 depletion had a less pronounced effect on the H2BK120$_{ub}$-stimulated histone mark H3K79$_{me2}$ [28-33] (Fig. 4A-B), possibly due to the long half-life of this mark [53] or H2B-K120$_{ub}$-independent H3K79 methylation pathways.

Previous work revealed that the PAF1C subunit PAF1 is required for transcription restart after UV irradiation [20]. Furthermore, it was found that RNAPII stably interacts with five PAF1C subunits (CTR9, PAF1, CDC73, PAF1 and SKI8), but not with RTF1, in response to UV-induced DNA damage [20]. While PAF1 and RTF1 are part of the same complex in yeast, RTF1 does not stably associate with PAF1C in human cells [22,34,54]. Therefore, we hypothesized that these subunits may have different contributions to transcription restart. In line with previous results using siRNAs or a degron system to deplete PAF1 in U2OS cells [20], we found that acute knockout of PAF1 by transfection of crPAF1 in RPE1 cells impaired transcription restart after UV irradiation (Fig 4C-D). To test whether this is a general feature of the PAF1 core complex, we performed an acute knockout of another core subunit, CTR9, which similarly impaired transcriptional restoration (Fig. 4C–D). In contrast, acute knockout of RTF1, which was confirmed by western blot analysis, did not affect transcription recovery (Fig 4C-D), suggesting that RTF1 is dispensable for this process. Together, our findings show that core PAF1C proteins, but the not dissociable subunit RTF1 drives transcription restoration after UV in a manner that is not mediated via H3K79$_{me2}$, H2B-K120$_{ub}$ or H3K4$_{me3}$ deposition.

To study the relationship between PAF1C binding to RNAPII in more detail, we employed co-immunoprecipitation, which is better suited for detecting DNA damage-specific interactions, and proximity labeling, which is more appropriate for capturing transient binding of elongation factors to RNAPII during unperturbed transcription. Co-immunoprecipitation of RNAPII-S2 from UV-irradiated cells showed that the interaction of PAF1, but not RTF1, with RNAPII is enhanced by UV damage in a CSB-dependent manner (Fig 4E). Our co-immunoprecipitation approach fails to detect PAF1 or RTF1 interactions with RNAPII in undamaged conditions, while these are well described interactions [34]. As mentioned, this is likely because the interactions are too transient and therefore not detected using our IP

approach. Proximity labelling methods, such as those using biotin ligase UltraID, allow detection of transient protein-protein interactions [55]. To study transient interactions of elongating RNAPII, we endogenously fused UltraID to elongation factor ELOF1 using a knock-in approach [5,7]. As a control, we knocked UltraID into the ELOF1 locus, flanked by a T2A peptide that causes ribosome skipping during translation and thereby produces two separate proteins, ELOF1 and UltraID, from a single mRNA transcript. Indeed, this proximity-labelling approach showed that PAF1C interacts with elongating RNAPII in the absence of DNA damage (Fig 4F), as expected, while no interactions were detected with the UltraID only control. Importantly, the interaction of PAF1C with elongating RNAPII is independent of CSB (Fig 4F). Together, these findings indicate that DNA damage induces a CSB-dependent stabilization in the interaction between PAF1C and RNAPII, which is likely central to the transcription restart function of PAF1C.

Together, we demonstrated that the PAF1C elongation complex contributes to transcription restart after DNA damage, independently of the RTF1 subunit and in a manner that does not correlate with or depend on transcription-associated histone marks H3K79$_{me2}$, H2B-K120$_{ub}$ and H3K4$_{me3}$.

Discussion

Our study demonstrates that initial post-repair transcription restart is independent of histone modifications H2B-K120$_{Ub}$, H3K4$_{me3}$ and H3K79$_{me2}$. While these marks correlate with active transcription, they are not strictly required for transcription [45 41 56 57 58]. Our data indicates that RNA synthesis can happen in the absence of these marks, both in unchallenged and post-repair conditions.

Previous studies in model systems other than human cells have shown that transcription restart after DNA damage partially depends on methylation of either H3K4 and H3K79. In *C. elegans*, H3K4 methylation and the SET1/COMPASS complex facilitate transcription restart after DNA damage[42], whereas our findings show that neither H3K4$_{me3}$ nor the SET1/COMPASS complex is required for transcription recovery in human cells. In line with our findings in human cells, in *C. elegans* only H3K4$_{me2,}$ but not H3K4$_{me3}$ dynamically changes in response to DNA damage [42]. H3K4$_{me2}$ and H3K4$_{me3}$ have different dynamics, genomic distributions and have at least partially non-overlapping functions [38,57,59]. Furthermore, H3K4 methyltransferases other than the SET1/COMPASS complex can contribute to H3K4$_{me2}$ deposition [42], potentially explaining interspecies differences. Moreover, in the *C. elegans* experimental set-up, L1 larvae are irradiated and followed during development until adulthood, suggesting that H3K4$_{me2}$ deposition may be a specific developmental response that we do not capture in cultured human cells [42].

In mouse embryonic fibroblasts, DOT1L-mediated H3K79 methylation has been reported to contribute to transcription restart [43], whereas we find no requirement for this modification in human cells. Similar to previously observed differences in TCR requirements between mouse and human cells [49], these findings may reflect interspecies differences in chromatin prerequisites for transcription recovery. We also note that DOT1L-deficient mouse cells were generated using a gene-trap insertion approach, and that the transcription restoration phenotype in these cells was not rescued by re-expression of DOT1L [43,60]. This would be a critical control to rule out off-target effects caused by the gene-trap insertion. A previous report in human cells identified a role for DOT1L in transcriptional restart at sites of

transcription-replication conflicts [61], suggesting dependency on DOT1L in transcription restart is damage and location specific.

Post-repair transcription restart can occur without histone mark deposition. Both PAF1 and CTR9, core subunits of the PAF1C transcription elongation complex are essential for efficient transcription restart, while the dissociable subunit RTF1 is dispensable. This finding is in line with the observation that RTF1 dissociates from RNAPII before CSB binding *in vitro* [62], while the other five subunits are stabilized on RNAPII after DNA damage *in vivo* [20]. Moreover, considering that RTF1 is essential for PAF1C-dependent histone modifications, this already suggests that the role of PAF1C in transcription recovery is independent of the deposition of these marks. Interestingly, RTF1 does contribute to RNAPII velocity [22], suggesting that not all transcription elongation factors are required for transcription restart. PAF1 may influence transcription restart via regulation of (RTF1-independent) transcription elongation [21,22,63] or promoter-proximal pause release [23,24,26]. In addition, PAF1C physically interacts with CSB [20,64], and the RNAPII interaction of PAF1 depends on CSB, suggesting this is a dedicated, TCR-specific pathway to activate post-repair transcription.

In conclusion, our study provides evidence that transcription recovery following genotoxic stress depends on PAF1C, but is independent of transcription-associated histone modifications and RTF1. It would be interesting to further dissect differences in specific requirements of post-repair restart compared to those of general transcription.

Figures Legends

Figure 1 | H3K79$_{me2}$ is dispensable for transcription restart after DNA damage

a. Western blot with indicated antibodies of WT and CSB-KO cells untreated or treated with 5 µM DOT1Li (pinometostat) for 7 days.
b. RNA recovery assay (RRS) of conditions from (a). Cells were EU labeling for 1h in unirradiated (mock) condition or 3 h and 24 h after 12 J/m^2 UV. Cells depicted as individual data points. Circles are individual means of three biological replicates. Lines indicate means. Scale bar, 10 µm.
c. Western blot of RPE1 cells with the indicated genotype.
d. Nascent RNA synthesis in nonirradiated cells relative to WT cells of cell from (c).
e. RRS as in (b) of cells from (c). Scale bar, 10 µm.

Figure 2 | H3K4$_{me3}$ is dispensable for transcription restart after DNA damage

a. Western blot of RPE1 cells 5 days after Cas9 induction and transfection with indicated crRNAs.
b. Representative images of cells labelled for 1h with EU, unirradiated, 3h and 24h after 12 J/m^2 UV, 6 days after transfection with indicated crRNAs. Scale bar, 10 µm.
c. Nascent EU incorporation in nonirradiated cells relative to WT cells of cells transfected with indicated crRNAs..
d. Quantification of H3K4$_{me3}$ levels in conditions from (b), normalized to crNC mock condition. Individual data points represent cells, circles represent means from biological replicates. Pink dots represent cells with relative H3K4$_{me3}$ levels below 0.2, numbers indicate percentage of cells with relative H3K4$_{me3}$ levels below 0.2
e. Quantification of EU levels in conditions from (b), normalized to the mock condition per crRNA.

Figure 3 | H2BK120$_{Ub}$ is dispensable for transcription restart after DNA damage

a. Western blot of RPE1 cells 5 days after Cas9 induction and transfection with indicated crRNAs.
b. Representative images of cells labelled for 1h with EU, unirradiated or 3 h and 24h after 12 J/m^2 UV, 6 days after transfection with indicated crRNAs. Scale bar, 10 µm.
c. Nascent EU incorporation in nonirradiated cells relative to WT cells of cells transfected with indicated crRNAs.
d. Quantification of H2B-K120$_{Ub}$ levels in conditions from (b), normalized to crNC mock condition. Individual data points represent cells, circles represent means from biological replicates. Pink cells are cells with relative H2B-K120$_{Ub}$ levels below 0.2, numbers indicate percentage of cells with relative H2B-K120$_{Ub}$ levels below 0.2.
e. Quantification of EU levels in conditions from (b), as in (c) but normalized to mock condition per crRNA.

Fig 4 | RTF1 is not required for transcription restart

a. Western blot of RPE1 cells 5 days after Cas9 induction and transfection with indicated crRNAs.

b. Quantifications of western blots of H2B-K120Ub (left), H3K4me3 (middle) and H3K79me2 (right) levels, normalized to loading control tubulin and relative to crNC.

c. Representative images from RRS assay of cells 6 days after transfection with indicated crRNAs.

d. RRS of conditions from (c). Cells were EU labelled for 1h in cells unirradiated, 3 h and 24 h after 12 J/m^2 UV. Cells are depicted as individual data points. Circles are individual means of three biological replicates. Lines indicate means. Scale bar, 10 µm.

e. RNAPII-S2 co-immunoprecipitation in unirradiated (-) or 1h after 12J/m^2 UV irradiation in WT and CSB^{KO} cells.

f. ELOF1-UltraID proximity biotin-labelled proteins were streptavidin precipitated followed by detection with western blot. ELOF1-T2A-UltraID (right lane) is a negative control.

Acknowledgments

MSL laboratory was supported by the European Research Council Consolidator Grant STOP-FIX-GO (grant agreement No 101043815) and the Netherlands Scientific Organization (NWO) Vici grant (VI.C.212.005). The funders had no role in study design, data collection and analysis, the decision to publish, or the preparation of the manuscript.

Data Availability

This published article (and its supplementary information files) includes all data generated or analyzed during this study.

Competing interests

The authors declare no competing interests.

Author contribution

JJMvS generated knockouts; performed RRS experiments, immunofluorescence for histone marks, western blots for knockouts and histone marks, and co-immunoprecipitation; prepared figures; and wrote the paper. BAFJdG generated and validated ELOF1-UltraID cells and controls, performed proximity labeling coupled with western blotting, and prepared figures. MSL supervised the project, acquired funding, and wrote the paper.

Methods

Cell lines and cultures

The RPE1 cell lines were cultured at 37°C in an atmosphere of 5% CO_2 in DMEM GlutaMAX (Thermo Fisher Scientific) supplemented with penicillin/streptomycin (Sigma), and 8% fetal bovine serum (FBS; Bodinco BV or Thermo Fischer Scientific (Gibco)).

Generation of knockout cells

Parental RPE1-hTERT cells stably expressing inducible Cas9 (iCas9) that are also knockout for TP53 and the puromycin-N-acetyltransferase PAC1 gene were described previously (referred to as RPE1-iCas9). To generate knockouts in RPE1-iCas9, one day after induction of Cas9 by addition of 200 ng/ul doxycline (Clontech, 8634-1), cells were transfected with 10nM crRNA:tracrRNA duplexes using 1:1000 Lipofectamine RNAimax transfection reagent (Invitrogen, 13778150). crRNAs in Supplementary Table 2. Two days after transfection, single cells were plated by limiting dilution. After single cell clone expansion, clones were selected by western blot and Sanger sequencing using the oligos listed in Supplementary Table 4.

Western blotting

Total cell lysates were harvested by scraping cells in the Laemmli-SDS sample buffer. Chromatin fractions were obtained by lysing cell pellets on ice in EBC-1 buffer (50 mM Tris [pH 7.5], 150 mM NaCl, 2 mM MgCl2, 0.5% NP-40, and protease inhibitor cocktail (Roche)) for 20 min at 4° C, on a rotating wheel followed by centrifugation and removal of the supernatant. Chromatin pellets were resuspended in the Laemmli-SDS sample buffer. Total cell lysates or chromatin fraction samples were boiled for 10 min at 95°C. Proteins were separated on Criterion™ XT Tris-Acetate 3–8% Protein Gels (BioRad, #3450131) in Tris/Tricine/SDS Running Buffer (BioRad, #1610744) or on Criterion Xt bis-tris 4-12% gels in MOPS running buffer. Then, blotted onto PVDF membranes (IPFL00010, EMD Millipore) in Tris/glycine blotting buffer (0.025 M Tris, 0.192 M glycine) with 20% methanol. Membranes were blocked with 5% fat-free milk in PBS with 0.1 % Tween-20 for 1 h at room temperature. Membranes were then probed with indicated antibodies in 5% fat-free milk in PBS with 0.1 % Tween-20 (Antibodies are listed in Supplementary Table 5). Proteins were stained with fluorochrome-conjugated secondary antibodies and were detected on an Odyssey CLx system and Image Studio software (Li-Cor).

Recovery of RNA synthesis (RRS)

After irradiation with UV-C light (12 J/m2), cells were allowed to recover for indicated times followed by pulse labelling with 400 µM 5-ethynyl-uridine (EU; Jena Bioscience) for 1 h. Next, cells were medium chased with DMEM without supplements followed by fixation in 3.7% paraformaldehyde in PBS for 15 min. Cells were permeabilized with 0.5% Triton X-100 for 10 min and blocked in 1.5% bovine serum albumin (BSA, Thermo Fisher) in PBS. Nascent EU labelled RNA was visualized by click-it chemistry, by incubating the cells with 60 µM Atto azide-Alexa 594 (Atto Tec), 4 mM copper sulfate (Sigma), 10 mM ascorbic acid (Sigma) and 0.1 µg/mL DAPI in 50 mM Tris-buffer pH 8 for 1 h. After washing extensively with PBS, slides were mounted in Polymount (Brunschwig).

Microscopic analysis of fixed cells

Images of fixed samples were acquired on a Zeiss AxioImager M2 widefield fluorescence microscope equipped with 63x PLAN APO (1.4 NA) oil-immersion objectives (Zeiss) and an HXP 120 metal-halide lamp used for excitation. Fluorescent probes were detected using the following filters for DAPI (excitation filter: 350/50 nm, dichroic mirror: 400 nm, emission filter: 460/50 nm) , Alexa 555/594 (excitation filter: 545/25 nm, dichroic mirror: 565 nm, emission filter: 605/70 nm), or Alexa 647 (excitation filter: 640/30 nm, dichroic mirror: 660 nm, emission filter: 690/50 nm). Images were recorded using ZEN 2012 software (blue edition, version 1.1.0.0) and analyzed in Image J (1.48v).

Generation of ELOF1-UltraID cells

To generate endogenous knock-ins of UltraID-TY or T2A-UltraID-TY into the ELOF1 locus, RPE1-iCas9 WT and CSB-KO (1-15) cells were cultured in 6 cm plates prior to transfection. To promote homology-directed repair, cells were pretreated with PolQ inhibitor (ART558, MCE, 10 µM) and DNA-PK inhibitor (NU7441, MCE, 2 µM) 24 hours before transfection. RPE1 WT or CSB-KO (1-15) cells were then transfected with plasmids encoding a single guide RNA (sgRNA) targeting ELOF1, a Cas9-GFP construct (pML#187), and knock-in plasmids containing 1 kb homology arms targeting the ELOF1 locus, either ELOF1-UltraID-TY-T2A-Puromycin (pML#355) or T2A-UltraID-TY-T2A-Puromycin (pML#385), using 1 µg/µl PEI (Merck) in OptiMEM (Life Technologies, 51985034), followed by overnight incubation. Both plasmids (pML#355 and pML#385) contain a puromycin resistance cassette flanked by ~1 kb homology arms to enable selection. After overnight transfection, cells were cultured for 2–3 days in standard DMEM supplemented with PolQ (10 µM) and DNA-PK (2 µM) inhibitors. GFP-positive cells were subsequently sorted by FACS and seeded. Single clones were isolated, transferred to individual culture plates, and selected for ELOF1-UltraID knock-ins using 1 µg/ml puromycin. Genomic DNA was extracted, and successful knock-in of UltraID or T2A-UltraID at the ELOF1 locus was confirmed by Sanger sequencing following nested PCR amplification of genomic DNA.

Proximity labeling and streptavidin-based enrichment of biotinylated proteins

Cells were seeded and grown in 15 cm dishes until reaching 80% confluency. They were then incubated with 50 µM biotin for 15 minutes, followed by a 15-minute starvation in plain DMEM medium (Gibco, 31966-047). Subsequently, cells were collected by trypsinization and resuspended in 1× PBS at 4 °C. Immediately after resuspension, cells were pelleted by centrifugation at 1500 rpm and washed with 1× PBS. Cell pellets were snap-frozen in liquid nitrogen and stored at –80 °C until pull-down. Cells were lysed at 4 °C for 20 minutes using 1 ml of lysis buffer (50 mM Tris [pH 7.5], 150 mM NaCl, 0.1% deoxycholate, 2 mM $MgCl_2$, 0.5% NP-40, and protease inhibitor cocktail [Roche]) supplemented with 500 U/ml benzonase (Novagen). After lysis, the volume was adjusted to 2.5 ml with lysis buffer. To remove free biotin and cell debris, the protein lysate was processed using a G25/PD-10 size exclusion column (Cytiva, 17085101) according to the manufacturer's protocol. The resulting 3.5 ml protein eluate was incubated overnight at 4 °C with 30 µl streptavidin–sepharose beads (Merck Millipore, 69203-3) and 1000 U/ml benzonase to capture all biotin-labeled proteins. After six washes with washing buffer (50 mM Tris [pH 7.5], 300 mM NaCl, 0.1% deoxycholate, 1 mM EDTA, 0.5% NP-40), samples were boiled in 2× Laemmli buffer containing 0.2 mg/ml biotin and analyzed by western blot.

RNAPII-S2 co-immunoprecipitation

Where indicated, cells were irradiated with UV-C (12 J/m^2) and harvested 1 h after irradiation. Cells were lysed for 20 min at 4 C in 1 mL EBC-1 buffer (50 mM Tris [pH 7.5], 150 mM NaCl, 2 mM MgCl2, 0.5% NP-40, and protease inhibitor cocktail (Roche)), followed by collection of the chromatin-enriched pellet by centrifugation. Pellets were resuspended in EBC-1 buffer with 500 U/mL Benzonase Nuclease (Novagen) and 2 µg Pol II-S2 (ab5095, Abcam) 1 h at 4 °C. Next, the salt concentration was increased to 300 mM NaCl. Samples were incubated for an additional 30 min at 4 °C, followed by centrifugation at 14.000 x g. 50 µL of supernatant was mixed with 50 µL 2x Laemmli buffer as input sample. The remaining supernatant was incubated with 20 µL equilibrated Protein A agarose beads (Millipore) at 4 °C for 90 min (except for GFP-trap agarose incubated samples). Next, beads were washed 6 times with EBC-2 buffer (50 mM Tris, pH 7.5, 300 mM NaCl, 0.5% NP-40, 1 mM EDTA), and boiled in Laemmli-SDS buffer, followed by analysis by western blot.

Supplementary Table 1: Cell lines

Cell lines	Source
RPE1-iCas9 (WT)	[5]
RPE1-iCas9 CSB-KO (1-15)	[5]
RPE1-iCas9 DOT1L-KO2	This study
RPE1-iCas9 DOT1L-KO6	This study
RPE1-iCas9 KI ELOF1-ultraID-TY #3	This study
RPE1-iCas9 KI ELOF1 T2A-ultraID-TY #4	This study
RPE1-iCas9 KI CSB-KO (1-15) ELOF1-UltraID #2-10	[5] and this study

Supplementary Table 2: crRNAs

crRNA	Sequence	Gene_ID
OR10A7 (NC)	TTTCTGTGGACCAAATGCCG	ENSG00000179919
DOT1L-2 (KO2)	CAGGCCGTGCACTCACCGGA	ENSG00000104885
DOT1L-6 (KO6)	GATATGGCGCAGGAGTCCAG	ENSG00000104885
CSA	GGAGAGCAGAGTCAACACGG	ENSG00000049167
RTF1	GCTCAGCTCACCTTCCTCAG	ENSG00000137815
PAF1	TGTGAAGCAGCAGTTTACCG	ENSG00000006712
CTR9_11	TAGCTGGAATACTACAAGCA	ENSG00000198730
CTR9_14	AAAGCATTGCGTACTAACCC	ENSG00000198730

Supplementary Table 3: Plasmids

Plasmid	Origin	Identifier
pML#355_H.Arm1_ELOF1_T2A_ultaID_H.Arm2	Addgene plasmid #72824	pML#355
pML#385_H.Arm1_T2A_ELOF_T2A_ultaID_H.Arm2	Addgene plasmid #72824	pML#385
pML#187_pX458-(Cas9-2A-GFP)-sgELOF1-3	Addgene plasmid #48138	pML#187

Supplementary Table 4: Oligos

Gene	Sequence	Identifier
ELOF1	CACCGTGATTGGATAGACGCCTGCG	OML#302_sgelof1-3a - sgRNA-ELOF1-Sense for cloning pml#187
	AAAC CGCAGGCGTCTATCCAATCA C	OML#303_sgelof1-3b - sgRNA-ELOF1-Antisense for cloning pml#187
	GCTGCGTGGTTTCCTCAAAC	OML#1217_ELOF1_seq_fw3 - conformation plasmid
	ATGTTGCCCAGGCTGGTATC	OML#320_sgelof1-2_Seq_FW - gDNA PCR
	CGGGAAGTCCAGTTGAGATG	OML#323_sgelof1-3_Seq_RV - gDNA PCR
	CACCGTGATTGGATAGACGCCTGCG	OML#302 – nested PCR gDNA ELOF1
	GCCACCGGTCCGCGGTTTAAACTTAAGCT	OML#674 – nested PCR gDNA ELOF1
	GCACAATTGGCATCAAGTAATCCTCTCACC TTAGCTTCCC	OML#693_homology_arm1_ELOF1
	GACGTCGACTCTGTGTCGTCTCTGATTGGC CGTCTCGCAGGC	OML#694_homology_arm1_ELOF1
	GCACGTACGACCCGCCCCCTGAGCAGCCC CGCGTACTGTGG	OML#695_homology_arm2_ELOF1
	GACCATATGGAAGGCCAGAGGTCAGCGTC TGGCTAGAGG	OML#696_homology_arm2_ELOF1
pMK286 backbone	CAGGAAACAGCTATGAC	OML#172_AID-N/B_flank2 Rv

Supplementary Table 5: Antibodies

Antibody	Host	Company (reference)	Use	Identifier
CSA/ERCC8	Rabbit	Abcam, #137033 (EPR9237)	WB: 1:1000	aML#028
α-Tubulin	Mouse	Sigma, #T6199 (DM1A)	WB: 1:1000	aML#008
HSPA4	Rabbit	Novus Biologicals, NBP1-81696	WB: 1:1000	aML#114
H3K4me$_3$	Rabbit	Cell Signaling, #9751S	WB: 1:1000 IF: 1:1000	aML#237
DOT1L	Rabbit	Cell Signaling, #77087 (D1W4Z)	WB: 1:1000	aML#216
H3K79me$_2$	Rabbit	Abcam, ab3594	WB: 1:1000	aML#227
H2B-K120$_{Ub}$	Rabbit	Cell Signaling, 5546S	WB: 1:1000 IF: 1:1000	aML#177
PAF1	Rabbit	Bethyl, A300-172A	WB: 1:3000	aML#022
RTF1	Rabbit	Bethyl, A300-178A	WB: 1:1000	aML#257
RNAPII	Rabbit	Bethyl, A304-405A	WB: 1:1000	aML#088
RNAPII-S2	Rabbit	Abcam, ab5095	IP: 1:250 WB: 1:1000	aML#024
SPT5	Mouse	Santa Cruz, sc-133217	WB: 1:1000	aML#122
CTR9	Rabbit	Bethyl, A301-395A	WB: 1:1000	aML#049
TY1	Mouse	Diagenode, C15200054	WB: 1:1000	aML#154
Rabbit Alexa 647	Goat	Thermo Fisher, A-21245	IF: 1:1000	aML#016
CF770 Goat Anti-Mouse IgG (H+L)	Goat	Biotium, VWR #20077	WB: 1:10000	aML#009
CF680 Goat Anti-Rabbit IgG (H+L),	Goat	Biotum, VWR#: 20067	WB: 1:10000	aML#010

References

1 Epanchintsev, A. *et al.* Cockayne's Syndrome A and B Proteins Regulate Transcription Arrest after Genotoxic Stress by Promoting ATF3 Degradation. *Mol Cell* **68**, 1054-1066 e1056 (2017). https://doi.org:10.1016/j.molcel.2017.11.009

2 Tufegdzic Vidakovic, A. *et al.* Regulation of the RNAPII Pool Is Integral to the DNA Damage Response. *Cell* **180**, 1245-1261 e1221 (2020). https://doi.org:10.1016/j.cell.2020.02.009

3 Proietti-De-Santis, L., Drane, P. & Egly, J. M. Cockayne syndrome B protein regulates the transcriptional program after UV irradiation. *EMBO J* **25**, 1915-1923 (2006). https://doi.org:10.1038/sj.emboj.7601071

4 Rockx, D. A. *et al.* UV-induced inhibition of transcription involves repression of transcription initiation and phosphorylation of RNA polymerase II. *Proc Natl Acad Sci U S A* **97**, 10503-10508 (2000). https://doi.org:10.1073/pnas.180169797

5 van der Weegen, Y. *et al.* ELOF1 is a transcription-coupled DNA repair factor that directs RNA polymerase II ubiquitylation. *Nat Cell Biol* **23**, 595-607 (2021). https://doi.org:10.1038/s41556-021-00688-9

6 van der Weegen, Y. *et al.* The cooperative action of CSB, CSA, and UVSSA target TFIIH to DNA damage-stalled RNA polymerase II. *Nat Commun* **11**, 2104 (2020). https://doi.org:10.1038/s41467-020-15903-8

7 Geijer, M. E. *et al.* Elongation factor ELOF1 drives transcription-coupled repair and prevents genome instability. *Nat Cell Biol* **23**, 608-619 (2021). https://doi.org:10.1038/s41556-021-00692-z

8 Kokic, G. *et al.* Structural basis for RNA polymerase II ubiquitylation and inactivation in transcription-coupled repair. *Nat Struct Mol Biol* **31**, 536-547 (2024). https://doi.org:10.1038/s41594-023-01207-0

9 Mevissen, T. E. T., Kummecke, M., Schmid, E. W., Farnung, L. & Walter, J. C. STK19 positions TFIIH for cell-free transcription-coupled DNA repair. *Cell* **187**, 7091-7106 e7024 (2024). https://doi.org:10.1016/j.cell.2024.10.020

10 Ramadhin, A. R. *et al.* STK19 drives transcription-coupled repair by stimulating repair complex stability, RNA Pol II ubiquitylation, and TFIIH recruitment. *Mol Cell* **84**, 4740-4757 e4712 (2024). https://doi.org:10.1016/j.molcel.2024.10.030

11 van den Heuvel, D. *et al.* STK19 facilitates the clearance of lesion-stalled RNAPII during transcription-coupled DNA repair. *Cell* **187**, 7107-7125 e7125 (2024). https://doi.org:10.1016/j.cell.2024.10.018

12 Laugel, V. *et al.* Mutation update for the CSB/ERCC6 and CSA/ERCC8 genes involved in Cockayne syndrome. *Hum Mutat* **31**, 113-126 (2010). https://doi.org:10.1002/humu.21154

13 Lehmann, A. R. DNA repair-deficient diseases, xeroderma pigmentosum, Cockayne syndrome and trichothiodystrophy. *Biochimie* **85**, 1101-1111 (2003). https://doi.org:10.1016/j.biochi.2003.09.010

14 Chiou, Y. Y., Hu, J., Sancar, A. & Selby, C. P. RNA polymerase II is released from the DNA template during transcription-coupled repair in mammalian cells. *J Biol Chem* **293**, 2476-2486 (2018). https://doi.org:10.1074/jbc.RA117.000971

15 Zhu, Y. *et al.* Coordination of transcription-coupled repair and repair-independent release of lesion-stalled RNA polymerase II. *Nat Commun* **15**, 7089 (2024). https://doi.org:10.1038/s41467-024-51463-x

16 Gonzalo-Hansen, C. *et al.* Differential processing of RNA polymerase II at DNA damage correlates with transcription-coupled repair syndrome severity. *Nucleic Acids Res* **52**, 9596-9612 (2024). https://doi.org:10.1093/nar/gkae618

17 van der Meer, P. J., Yakoub, G., Nakazawa, Y, Ogi, T. & Luijsterburg M.S. Clearance of DNA damage-arrested RNAPII is selectively impaired in Cockayne syndrome cells. *BioRxiv* (2024).

18 Kristensen, U. *et al.* Regulatory interplay of Cockayne syndrome B ATPase and stress-response gene ATF3 following genotoxic stress. *Proc Natl Acad Sci U S A* **110**, E2261-2270 (2013). https://doi.org:10.1073/pnas.1220071110

19 Mandemaker, I. K., Vermeulen, W. & Marteijn, J. A. Gearing up chromatin: A role for chromatin remodeling during the transcriptional restart upon DNA damage. *Nucleus* **5**, 203-210 (2014). https://doi.org:10.4161/nucl.29085

20 van den Heuvel, D. *et al.* A CSB-PAF1C axis restores processive transcription elongation after DNA damage repair. *Nat Commun* **12**, 1342 (2021). https://doi.org:10.1038/s41467-021-21520-w

21 Hou, L. *et al.* Paf1C regulates RNA polymerase II progression by modulating elongation rate. *Proc Natl Acad Sci U S A* **116**, 14583-14592 (2019). https://doi.org:10.1073/pnas.1904324116

22 Zumer, K. *et al.* Two distinct mechanisms of RNA polymerase II elongation stimulation in vivo. *Mol Cell* **81**, 3096-3109 e3098 (2021). https://doi.org:10.1016/j.molcel.2021.05.028

23 Chen, F. X. *et al.* PAF1, a Molecular Regulator of Promoter-Proximal Pausing by RNA Polymerase II. *Cell* **162**, 1003-1015 (2015). https://doi.org:10.1016/j.cell.2015.07.042

24 Yu, M. *et al.* RNA polymerase II-associated factor 1 regulates the release and phosphorylation of paused RNA polymerase II. *Science* **350**, 1383-1386 (2015). https://doi.org:10.1126/science.aad2338

25 Chen, F. *et al.* Biochemical insights into Paf1 complex-induced stimulation of Rad6/Bre1-mediated H2B monoubiquitination. *Proc Natl Acad Sci U S A* **118** (2021). https://doi.org:10.1073/pnas.2025291118

26 Chen, F. X. *et al.* PAF1 regulation of promoter-proximal pause release via enhancer activation. *Science* **357**, 1294-1298 (2017). https://doi.org:10.1126/science.aan3269

27 Van Oss, S. B. *et al.* The Histone Modification Domain of Paf1 Complex Subunit Rtf1 Directly Stimulates H2B Ubiquitylation through an Interaction with Rad6. *Mol Cell* **64**, 815-825 (2016). https://doi.org:10.1016/j.molcel.2016.10.008

28 Fetian, T. *et al.* Paf1 complex subunit Rtf1 stimulates H2B ubiquitylation by interacting with the highly conserved N-terminal helix of Rad6. *Proc Natl Acad Sci U S A* **120**, e2220041120 (2023). https://doi.org:10.1073/pnas.2220041120

29 Krogan, N. J. *et al.* The Paf1 complex is required for histone H3 methylation by COMPASS and Dot1p: linking transcriptional elongation to histone methylation. *Mol Cell* **11**, 721-729 (2003). https://doi.org:10.1016/s1097-2765(03)00091-1

30 Wood, A., Schneider, J., Dover, J., Johnston, M. & Shilatifard, A. The Paf1 complex is essential for histone monoubiquitination by the Rad6-Bre1 complex, which signals for histone methylation by COMPASS and Dot1p. *J Biol Chem* **278**, 34739-34742 (2003). https://doi.org:10.1074/jbc.C300269200

31 Worden, E. J., Hoffmann, N. A., Hicks, C. W. & Wolberger, C. Mechanism of Cross-talk between H2B Ubiquitination and H3 Methylation by Dot1L. *Cell* **176**, 1490-1501 e1412 (2019). https://doi.org:10.1016/j.cell.2019.02.002

32 Valencia-Sanchez, M. I. *et al.* Structural Basis of Dot1L Stimulation by Histone H2B Lysine 120 Ubiquitination. *Mol Cell* **74**, 1010-1019 e1016 (2019). https://doi.org:10.1016/j.molcel.2019.03.029

33 Kim, J. *et al.* RAD6-Mediated transcription-coupled H2B ubiquitylation directly stimulates H3K4 methylation in human cells. *Cell* **137**, 459-471 (2009). https://doi.org:10.1016/j.cell.2009.02.027

34 Francette, A. M., Tripplehorn, S. A. & Arndt, K. M. The Paf1 Complex: A Keystone of Nuclear Regulation Operating at the Interface of Transcription and Chromatin. *J Mol Biol* **433**, 166979 (2021). https://doi.org:10.1016/j.jmb.2021.166979

35 Gates, L. A., Foulds, C. E. & O'Malley, B. W. Histone Marks in the 'Driver's Seat': Functional Roles in Steering the Transcription Cycle. *Trends Biochem Sci* **42**, 977-989 (2017). https://doi.org:10.1016/j.tibs.2017.10.004

36 Zhang, T., Cooper, S. & Brockdorff, N. The interplay of histone modifications - writers that read. *EMBO Rep* **16**, 1467-1481 (2015). https://doi.org:10.15252/embr.201540945

37 Hu, S. *et al.* H3K4me2/3 modulate the stability of RNA polymerase II pausing. *Cell Res* **33**, 403-406 (2023). https://doi.org:10.1038/s41422-023-00794-3

38 Wang, H. *et al.* H3K4me3 regulates RNA polymerase II promoter-proximal pause-release. *Nature* **615**, 339-348 (2023). https://doi.org:10.1038/s41586-023-05780-8

39 Jeusset, L. M. & McManus, K. J. Characterizing and exploiting the many roles of aberrant H2B monoubiquitination in cancer pathogenesis. *Semin Cancer Biol* **86**, 782-798 (2022). https://doi.org:10.1016/j.semcancer.2021.12.007

40 Mattiroli, F. & Penengo, L. Histone Ubiquitination: An Integrative Signaling Platform in Genome Stability. *Trends Genet* **37**, 566-581 (2021). https://doi.org:10.1016/j.tig.2020.12.005

41 Ljungman, M., Parks, L., Hulbatte, R. & Bedi, K. The role of H3K79 methylation in transcription and the DNA damage response. *Mutat Res Rev Mutat Res* **780**, 48-54 (2019). https://doi.org:10.1016/j.mrrev.2017.11.001

42 Wang, S., Meyer, D. H. & Schumacher, B. H3K4me2 regulates the recovery of protein biosynthesis and homeostasis following DNA damage. *Nat Struct Mol Biol* **27**, 1165-1177 (2020). https://doi.org:10.1038/s41594-020-00513-1

43 Oksenych, V. *et al.* Histone methyltransferase DOT1L drives recovery of gene expression after a genotoxic attack. *PLoS Genet* **9**, e1003611 (2013). https://doi.org:10.1371/journal.pgen.1003611

44 Mao, P., Meas, R., Dorgan, K. M. & Smerdon, M. J. UV damage-induced RNA polymerase II stalling stimulates H2B deubiquitylation. *Proc Natl Acad Sci U S A* **111**, 12811-12816 (2014). https://doi.org:10.1073/pnas.1403901111

45 Cao, K. *et al.* DOT1L-controlled cell-fate determination and transcription elongation are independent of H3K79 methylation. *Proc Natl Acad Sci U S A* **117**, 27365-27373 (2020). https://doi.org:10.1073/pnas.2001075117

46 Wu, A. *et al.* DOT1L complex regulates transcriptional initiation in human erythroleukemic cells. *Proc Natl Acad Sci U S A* **118** (2021). https://doi.org:10.1073/pnas.2106148118

47 Ho, L. L. *et al.* DOT1L-mediated H3K79 methylation in chromatin is dispensable for Wnt pathway-specific and other intestinal epithelial functions. *Mol Cell Biol* **33**, 1735-1745 (2013). https://doi.org:10.1128/MCB.01463-12

48 Bernt, K. M. *et al.* MLL-rearranged leukemia is dependent on aberrant H3K79 methylation by DOT1L. *Cancer Cell* **20**, 66-78 (2011). https://doi.org:10.1016/j.ccr.2011.06.010

49 Apelt, K. *et al.* Human HMGN1 and HMGN2 are not required for transcription-coupled DNA repair. *Sci Rep* **10**, 4332 (2020). https://doi.org:10.1038/s41598-020-61243-4

50 Farooq, Z., Banday, S., Pandita, T. K. & Altaf, M. The many faces of histone H3K79 methylation. *Mutat Res Rev Mutat Res* **768**, 46-52 (2016). https://doi.org:10.1016/j.mrrev.2016.03.005

51 Barth, T. K. & Imhof, A. Fast signals and slow marks: the dynamics of histone modifications. *Trends Biochem Sci* **35**, 618-626 (2010). https://doi.org:10.1016/j.tibs.2010.05.006

52 Jiang, H. The complex activities of the SET1/MLL complex core subunits in development and disease. *Biochim Biophys Acta Gene Regul Mech* **1863**, 194560 (2020). https://doi.org:10.1016/j.bbagrm.2020.194560

53 Chory, E. J. *et al.* Nucleosome Turnover Regulates Histone Methylation Patterns over the Genome. *Mol Cell* **73**, 61-72 e63 (2019). https://doi.org:10.1016/j.molcel.2018.10.028

54 Francette, A. M. & Arndt, K. M. Multiple direct and indirect roles of the Paf1 complex in transcription elongation, splicing, and histone modifications. *Cell Rep* **43**, 114730 (2024). https://doi.org:10.1016/j.celrep.2024.114730

55 Kubitz, L. *et al.* Engineering of ultraID, a compact and hyperactive enzyme for proximity-dependent biotinylation in living cells. *Commun Biol* **5**, 657 (2022). https://doi.org:10.1038/s42003-022-03604-5
56 Wang, E. *et al.* Histone H2B ubiquitin ligase RNF20 is required for MLL-rearranged leukemia. *Proc Natl Acad Sci U S A* **110**, 3901-3906 (2013). https://doi.org:10.1073/pnas.1301045110
57 Wang, H. & Helin, K. Roles of H3K4 methylation in biology and disease. *Trends Cell Biol* **35**, 115-128 (2025). https://doi.org:10.1016/j.tcb.2024.06.001
58 Fetian, T., Grover, A. & Arndt, K. M. Histone H2B ubiquitylation: Connections to transcription and effects on chromatin structure. *Biochim Biophys Acta Gene Regul Mech* **1867**, 195018 (2024). https://doi.org:10.1016/j.bbagrm.2024.195018
59 Pinskaya, M. & Morillon, A. Histone H3 lysine 4 di-methylation: a novel mark for transcriptional fidelity? *Epigenetics* **4**, 302-306 (2009). https://doi.org:10.4161/epi.4.5.9369
60 Steger, D. J. *et al.* DOT1L/KMT4 recruitment and H3K79 methylation are ubiquitously coupled with gene transcription in mammalian cells. *Mol Cell Biol* **28**, 2825-2839 (2008). https://doi.org:10.1128/MCB.02076-07
61 Werner, M. *et al.* Transcription-replication conflicts drive R-loop-dependent nucleosome eviction and require DOT1L activity for transcription recovery. *Nucleic Acids Res* **53** (2025). https://doi.org:10.1093/nar/gkaf109
62 Kokic, G., Wagner, F. R., Chernev, A., Urlaub, H. & Cramer, P. Structural basis of human transcription-DNA repair coupling. *Nature* **598**, 368-+ (2021). https://doi.org:10.1038/s41586-021-03906-4
63 Rondon, A. G., Gallardo, M., Garcia-Rubio, M. & Aguilera, A. Molecular evidence indicating that the yeast PAF complex is required for transcription elongation. *EMBO Rep* **5**, 47-53 (2004). https://doi.org:10.1038/sj.embor.7400045
64 Tiwari, V., Kulikowicz, T., Wilson, D. M., 3rd & Bohr, V. A. LEO1 is a partner for Cockayne syndrome protein B (CSB) in response to transcription-blocking DNA damage. *Nucleic Acids Res* **49**, 6331-6346 (2021). https://doi.org:10.1093/nar/gkab458

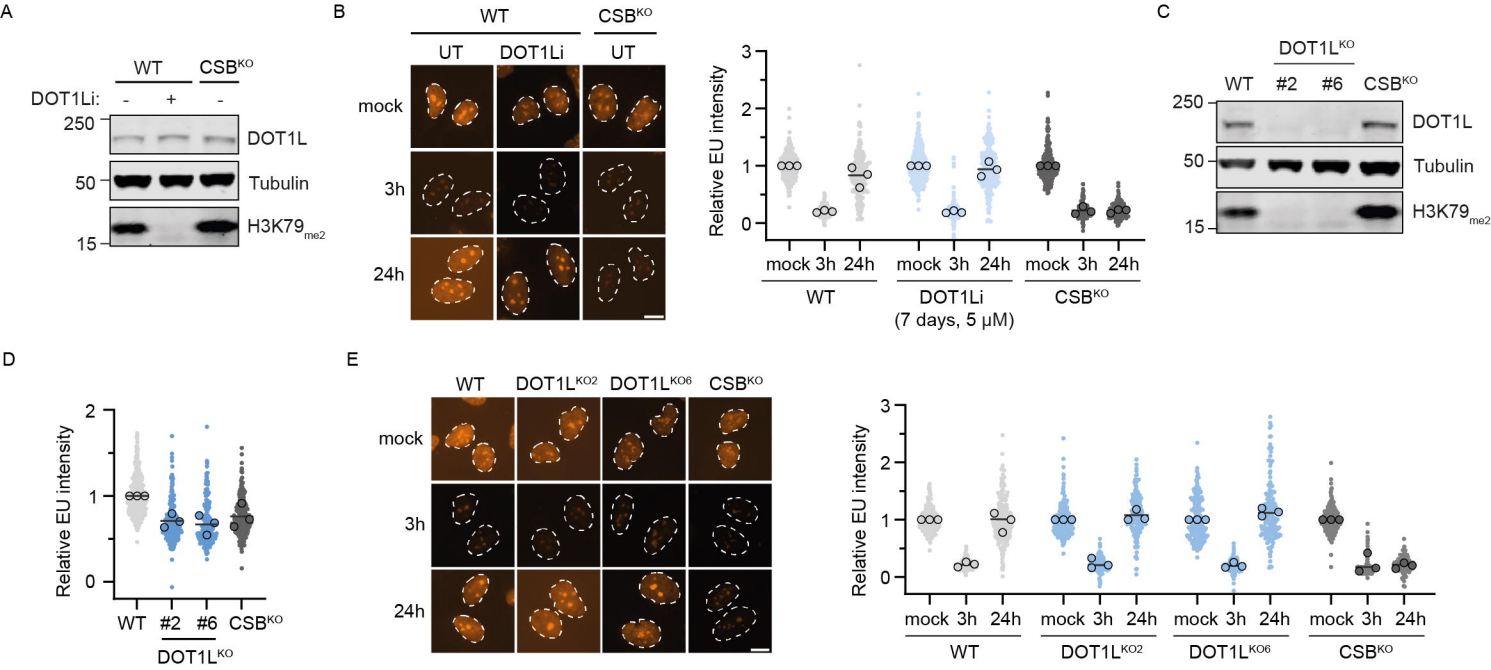
A
WT
CSB^KO
DOT1Li:
-
+
-
250
50
15
DOT1L
Tubulin
H3K79me2
B
WT
CSB^KO
UT
DOT1Li
UT
mock
3h
24h
Relative EU intensity
mock 3h 24h
WT
DOT1Li
(7 days, 5 μM)
CSB^KO
C
DOT1L^KO
WT
#2
#6
CSB^KO
DOT1L
Tubulin
H3K79me2
D
Relative EU intensity
WT
#2
#6
CSB^KO
DOT1L^KO
E
WT
DOT1L^KO2
DOT1L^KO6
CSB^KO
mock
3h
24h
Relative EU intensity
mock 3h 24h
WT
DOT1L^KO2
DOT1L^KO6
CSB^KO

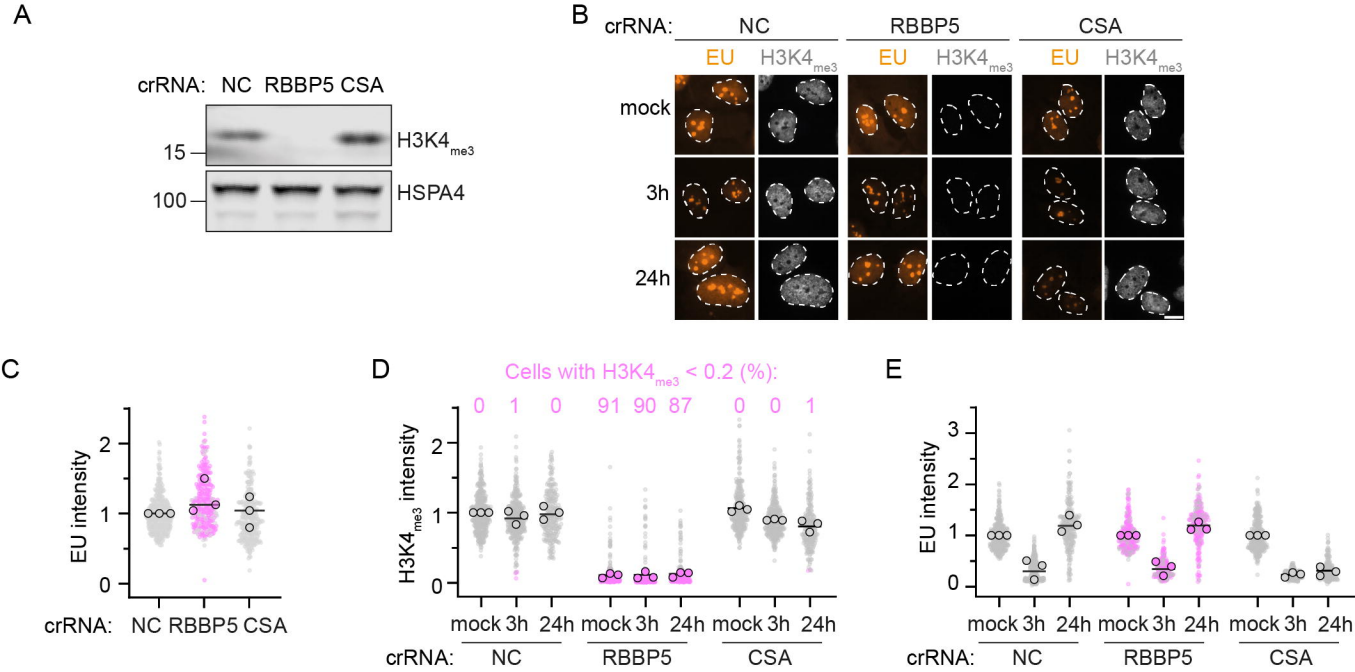
A
crRNA: NC RBBP5 CSA
15
100
H3K4me3
HSPA4
B
crRNA: NC RBBP5 CSA
EU H3K4me3 EU H3K4me3 EU H3K4me3
mock
3h
24h
C
EU intensity
crRNA: NC RBBP5 CSA
D
Cells with H3K4me3 < 0.2 (%):
0 1 0 91 90 87 0 0 1
H3K4me3 intensity
mock 3h 24h mock 3h 24h mock 3h 24h
crRNA: NC RBBP5 CSA
E
EU intensity
mock 3h 24h mock 3h 24h mock 3h 24h
crRNA: NC RBBP5 CSA

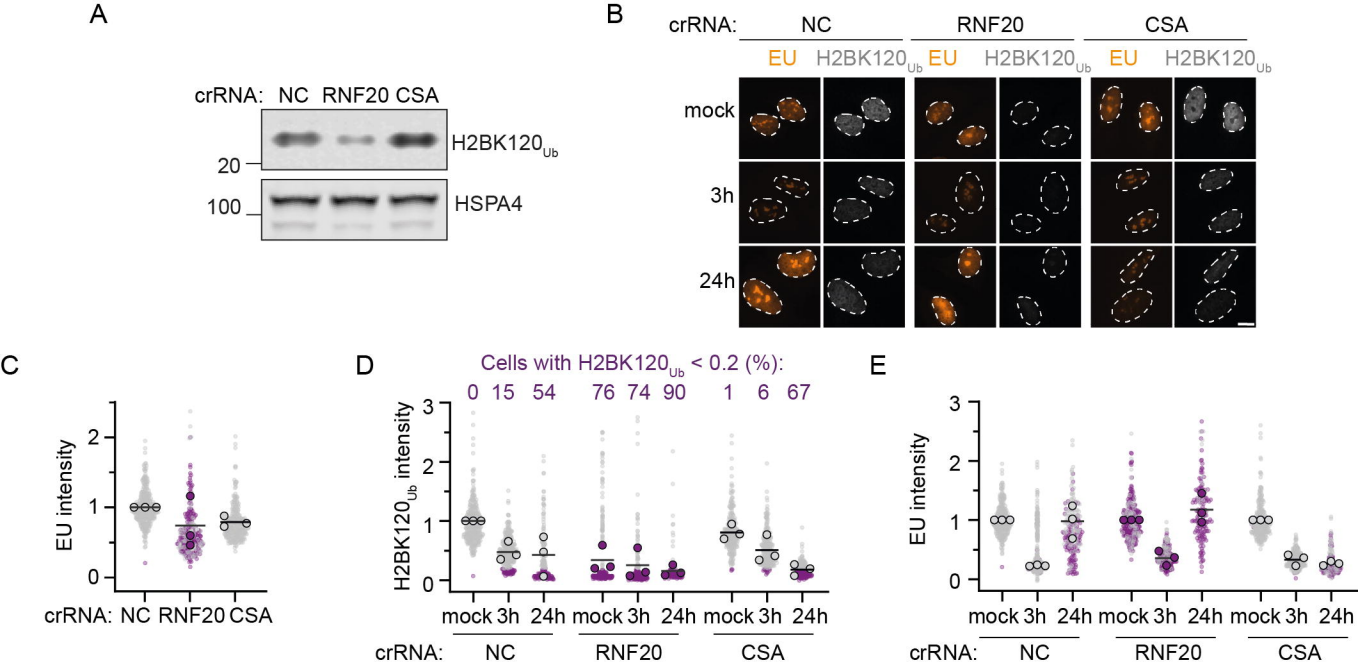
A
crRNA: NC RNF20 CSA
20
100
H2BK120Ub
HSPA4
B
crRNA: NC RNF20 CSA
EU H2BK120Ub EU H2BK120Ub EU H2BK120Ub
mock
3h
24h
C
EU intensity
crRNA: NC RNF20 CSA
D
Cells with H2BK120Ub < 0.2 (%):
0 15 54 76 74 90 1 6 67
H2BK120Ub intensity
mock 3h 24h mock 3h 24h mock 3h 24h
crRNA: NC RNF20 CSA
E
EU intensity
mock 3h 24h mock 3h 24h mock 3h 24h
crRNA: NC RNF20 CSA

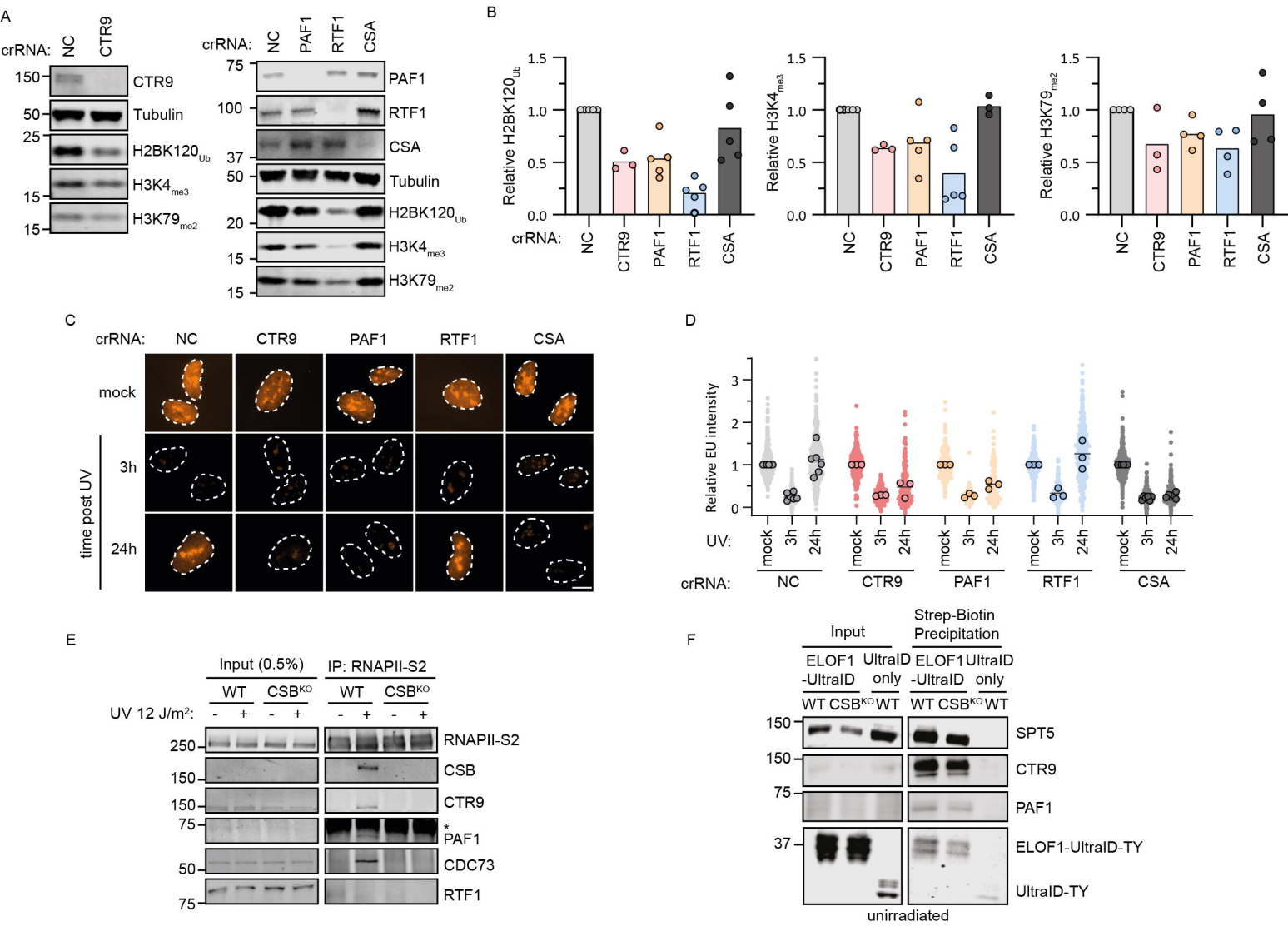
A
crRNA: NC CTR9
150 CTR9
50 Tubulin
25 H2BK120Ub
15 H3K4me3
15 H3K79me2
crRNA: NC PAF1 RTF1 CSA
75 PAF1
100 RTF1
37 CSA
50 Tubulin
20 H2BK120Ub
15 H3K4me3
15 H3K79me2
B
Relative H2BK120Ub
Relative H3K4me3
Relative H3K79me2
1.5
1.0
0.5
0.0
crRNA: NC CTR9 PAF1 RTF1 CSA
C
crRNA: NC CTR9 PAF1 RTF1 CSA
mock
time post UV
3h
24h
D
Relative EU intensity
3
2
1
0
UV: mock 3h 24h mock 3h 24h mock 3h 24h mock 3h 24h mock 3h 24h
crRNA: NC CTR9 PAF1 RTF1 CSA
E
Input (0.5%)
IP: RNAPII-S2
WT CSBKO WT CSBKO
UV 12 J/m2: - + - + - + - +
250 RNAPII-S2
150 CSB
150 CTR9
75 * PAF1
50 CDC73
75 RTF1
F
Input
Strep-Biotin Precipitation
ELOF1 -UltraID
UltraID only
ELOF1 -UltraID
UltraID only
WT CSBKO WT WT CSBKO WT
150 SPT5
150 CTR9
75 PAF1
37 ELOF1-UltraID-TY
UltraID-TY
unirradiated